Fabrication of a Straight Canted Cosine-Theta Prototype Magnet for Hadron Therapy

Daniel Barna, Ernesto De Matteis, Todor Gusvitskii, Thibault Lecrevisse, Samuele Mariotto, Danilo Pedrini, Diego Perini, Marco Prioli, Lucio Rossi, *Fellow, IEEE*, Stefano Sorti, Fernando Toral, Riccardo U. Valente, and Javier Munilla

***Abstract*—Canted Cosine Theta magnets are a very promising layout for applications in small accelerator systems, for example for the gantries needed at hadron therapy facilities. A 1-meter-long, straight and combined function magnet demonstrator with 80 mm aperture diameter, 4 T central field and 5 T/m quadrupole component is under development in the framework of the European-funded project IFAST. The main purpose of this demonstrator is to develop competencies and expertise about the CCT layout and explore the possibility of implementing a combined function CCT magnet. The design has been reported elsewhere. This paper includes details about the fabrication of this demonstrator, describing the techniques and tooling used in each step: machining, winding, wax impregnation and assembly. Special attention is paid to the splices since the cable is a twisted rope of six NbTi wires around a central copper wire.**

***Index Terms*—Superconducting magnet, canted cosine-theta, medical accelerators, particle therapy.**

I. Introduction

PARTICLE beam therapy, particularly with heavy ions such as carbon, offers a highly targeted approach to tumor treatment, significantly reducing damage to surrounding healthy tissue compared to conventional X-ray therapy [1]. However, widespread adoption of ion therapy is limited by the substantial size, complexity, and cost of the accelerator systems, especially if rotating gantries are required for multi-angle beam delivery. Superconducting magnets present a promising solution, enabling more compact and lightweight gantry designs while maintaining high magnetic field performance. This article focuses on the manufacturing development of a combined-function superconducting magnet based on the Canted Cosine Theta (CCT) geometry, which integrates bending and focusing functions into a single magnet structure. The detailed design has already been reported [2] and the main properties are reproduced here in Table I for convenience. This work is being done in the framework of the European I.FAST project, while significant synergies are found with the European HITRIPLUS project [3], where a curved version of a CCT magnet is being produced.

Table I
Main Specifications

Parameters	Values	Units
Magnetic length	0.8	m
Bore diameter	80	mm
Rope insulated diameter	3.15	mm
Spar thickness	4.2 (inner), 6 (outer)	mm
Minimum rib thickness	0.4	mm
Total current	1540	A
Number of turns (each layer)	50	
Total rope length	844	m

Therefore, this paper summarizes the fabrication steps of a CCT dipole, paying special attention to some critical and/or innovative procedures aimed at finding a reliable and robust manufacturing scheme. Some additional information about the cable is also shown here in Fig. 1, which is important to understand some of the techniques to be described in this paper: The coil is made of 14 cables, each one being composed of 7 wires plus a double polyester braid to protect against insulation issues, a serious problem when dealing with such a complicated geometry as the ones of the former and the grooves.

II. Electromechanical Model

Former and coil geometries were modelled for every expected use case. Special attention was given to the stress and displacement values both at cold and cold plus nominal current conditions. The results for the energized step load are shown in Fig. 2. As expected from previous design work, no stress

Received 28 July 2025; revised 2 October 2025; accepted 21 November 2025. Date of publication 2 December 2025; date of current version 29 December 2025. This work was supported European Commission H2020-I.FAST under Grant 101004730. *(Corresponding author: J. Munilla.)*

Daniel Barna is with the Wigner Research Centre for Physics, 1121 Budapest, Hungary.

Ernesto De Matteis, Danilo Pedrini, Marco Prioli, and Riccardo U. Valente are with the Laboratory of Accelerators and Applied Superconductivity, National Institute for Nuclear Physics, 95125 Milan, Italy.

Todor Gusvitskii is with the Laboratory of Accelerators and Applied Superconductivity, National Institute for Nuclear Physics, 95125 Milan, Italy, and also with the Sapienza University of Rome, 00185 Rome, Italy.

Thibault Lecrevisse is with the Commissariat a l'energie Atomique et Aux Energies Alternatives, 91191 Saclay, France.

Samuele Mariotto, Lucio Rossi, and Stefano Sorti are with the Laboratory of Accelerators and Applied Superconductivity, National Institute for Nuclear Physics, 95125 Milan, Italy, and also with the Dipartimento di Fisica, Universitá degli Studi di Milano, 20122 Milan, Italy.

Diego Perini is with CERN, CH-1211 Geneva, Switzerland.

Fernando Toral and Javier Munilla are with the Centro de Investigaciones Energeticas Medioambientales y Tecnologicas, 28040 Madrid, Spain (e-mail: javier.munilla@ciemat.es).

Color versions of one or more figures in this article are available at https://doi.org/10.1109/TASC.2025.3639381.

Digital Object Identifier 10.1109/TASC.2025.3639381

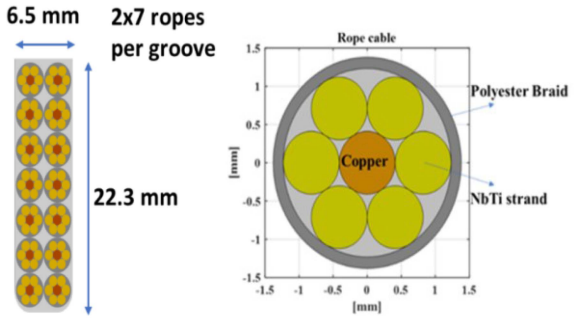

Fig. 1. Main specifications of the magnet (left). Schematics of the cable including wires and insulation (right).

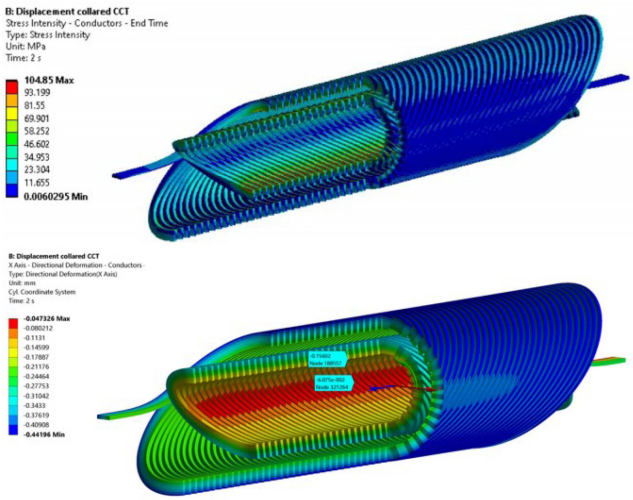

Fig. 2. Stress (up) and displacements (down) of the coils when modelled at cold and energized conditions inside the grooves with frictional contact.

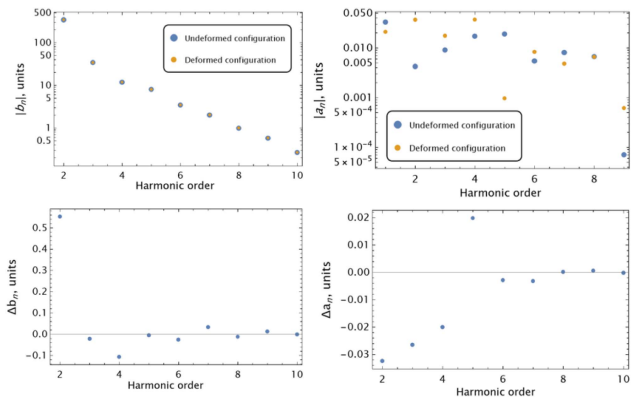

Fig. 3. Field quality values up to 10th harmonic considering the actual displacements when at cold and energized to nominal current.

concentrations are expected. Indeed, this is one of the key points of a CCT magnet, as the Lorentz force for each turn is independently supported, while in a conventional cosine theta magnet, the Lorentz forces are accumulated towards the main plane. On the other hand, in the canted option, there is a risk of high deformation of the coils if the walls between each groove are not stiff enough. The most common reason for a limitation in stiffness is to use thin walls. Moreover, this thickness is not constant because of the spatial twisting of the cables along their path, which will result in a local spot of minimum material

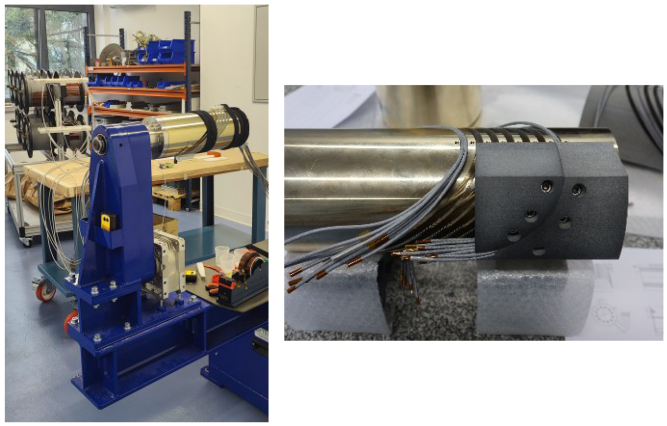

Fig. 4. (Left) Winding machine (front) and spools holder (back) with mockup former. (Right) Mockup of layer jump test.

between turns. Under these assumptions, the actual geometry of the whole former was modeled looking for both peak stress and peak deformation of the coils.

First, the stresses and displacements after cooling to nominal temperature were evaluated in ANSYS, including the whole former, the groove geometry and the coils with frictional contacts in between. In parallel, the Lorentz forces in the coils were evaluated using COMSOL so that these forces were transferred to the second load step in the ANSYS mechanical model. Therefore, a complete check of the stresses and the displacements at any condition was performed. In addition, the effect of such displacements in the field quality was studied using RAT software. This analysis is summarized in Fig. 3. These charts show the variation of the multipoles of the deformed model compared to the nominal one.

III. Winding Tests

In order to minimize the manufacturing risks, a winding test was conducted with a mockup former. This former was manufactured with the same diameter and grooves as the actual one, but significantly shorter (reduced number of turns). The cables used in this test were selected according to the same scheme, but made of Cu. The same insulation and outer diameter were selected. Also, the tooling for the spools, the winding machine and handling tooling designed for the superconducting magnet were used in this test.

The procedure for the winding was then optimized, and experience was gained prior to the superconducting cables usage. The parts for the layer jump were manufactured with a 3D FDM printer for this testing setup.

Some of the most important steps are shown in Figs. 4 and in Fig. 5. First, a conventional winding machine was used (Fig. 4, left). As this mockup is short, one support is enough. For the real-size one, two supports are required, one at each side. The support structure for the spools is also shown in the back. Given the relatively stiff nature of the group of cables to be handled, the spools are located far away (2 meters) to avoid additional tension. Guiding and positioning parts made of POM are therefore needed along the path, to progressively guide them

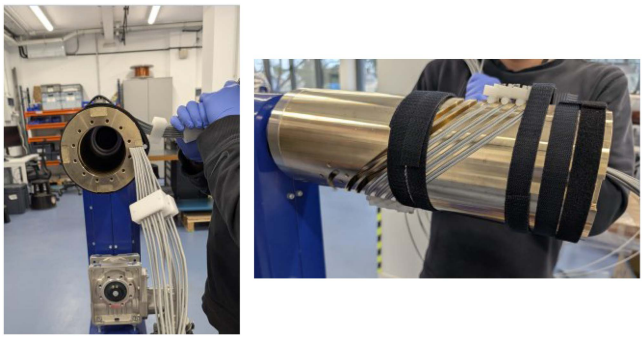

Fig. 5. (left) positioning of the cables into the grooves (right) detail of the clamping system of the cables.

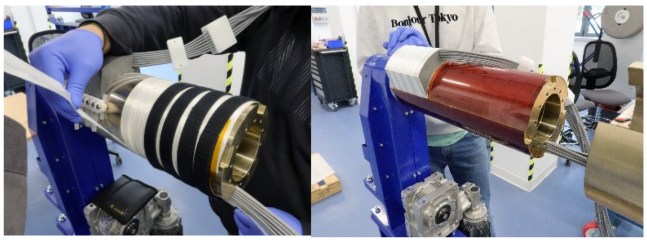

Fig. 6. (Left) insulation wrapping (right) outer layer positioning prior to assembly.

into the desired pattern with low friction (friction could damage the insulation).

Smooth-controlled movement of roll axis (rotation around longitudinal axis) is also required, so that the operator can gently guide the cables into the groove while the former is rotating (Fig. 5, left). In the event of any sign of blocking or excessive friction, the movement can be stopped or even reversed quickly. If there is too much friction on the cables, or this friction is not constant along the 14 cables, it is very difficult to properly guide all the cables to follow the curved path, so some clearance was found to be mandatory in all the guiding tools. Once each turn is in its position, custom clamps are placed to hold the cables in the groove. They cannot be removed until the full turn is ready for the insulation layers (Fig. 5, right).

In the case of the first layer, the layer jump parts must be installed at this moment, and the cables must already be placed in between them. During the winding, insulation between the cables and the former was checked. The design of the ropes with a double layer of polyester proved to be a robust option against insulation damage for this complex geometry.

Once the layer is completed (including the layer jump for the first layer), the insulation is to be installed (Fig. 6). First, a layer of fiber-glass fabric is rolled around the whole former with a 50% overlap. Second, a polyimide layer is placed. This polyimide layer was previously cut according to the layer jump shape.

One of the most delicate steps along this manufacturing procedure is the one when the second layer former is placed over the inner former. This is particularly important for the real-size magnet, where the distance is higher. In this procedure, it is important to provide a smooth and controlled way to control the movements of the outer former. The effective clearance is limited not only to the nominal dimensions, but also to the tolerances of every part and the insulation thickness after rolling. Moreover,

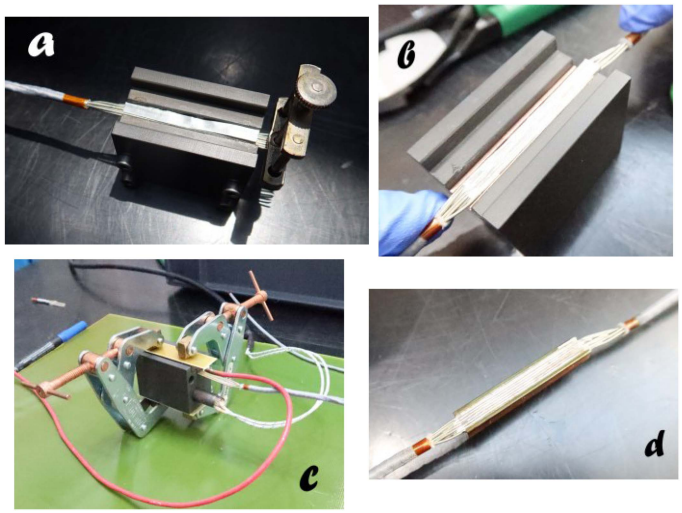

Fig. 7. (a) Pre-tinning of one cable (b) placing both cables for soldering. (c) Closed mold with probes. (d) Final splice.

the angular position of the former must be well controlled, as the layer jump is already prepared in advance, and the angular clearance is also limited. In fact, a suitable design with proper insulation but absolutely no gaps between the layer jump, the insulation and the outer former could not be found. These small volumes, located where no effect on the cables can be foreseen, will be filled with the impregnation wax in a later step.

IV. Splices Testing

Optimized splices are considered as one of the most important aspects for the overall performance of this magnet. They will introduce a resistive path for the current, and so a localized heat load, which could be remarkable as the current will cross 13 splices along the magnet because the 14 cables are connected in series. There is also a constraint for the volume occupied by the splices, which should be as small as possible for an optimized design.

In the case of the splices, a mockup test was carried out. The overall concept was adapted from previous experiences [4] in similar splices, and its main steps are shown in Fig. 7. The first step includes the insulation removal of the cable. The strands are then aligned in flat position. Both cables are then, separately, pre-tinned with a eutectic AgSn foil inside a heated mold (Fig. 7(a)). In the picture, the mold is ready to be closed and heated. Once both cables are pre-tinned (Fig. 7(b)), they can be placed inside the mold with a machined Cu plate to give mechanical strength and thermal homogeneity to the splice. A hand-shake approach is followed in these splices, which should be better in terms of resistance but also it is the convenient scheme for the specific geometry of this magnet, where the two terminals to be soldered are coming out from the formers in opposite angular positions. More information about the concept of these splices and their performance can be found at [5].

The mold itself includes two drills close to, but not in contact with, to the soldering volume where the cable is to be placed: One for the heating element and the other for a thermocouple probe. A PID control system controls the heating power to be above the 221 °C eutectic temperature. Grips are placed around

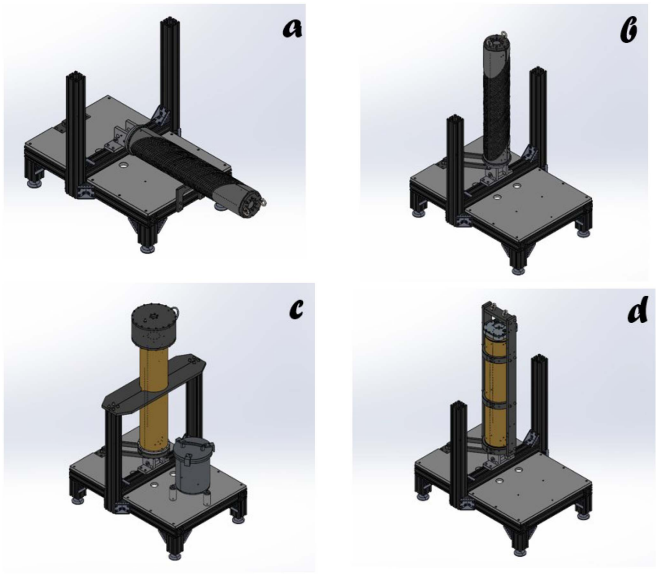

Fig. 8. (a) Winding finished coming from winding machine (b) magnet tilted. (c) Impregnation step (d) Transportation structure.

this mold to keep the proper position along the whole procedure (Fig. 7(c)). Once the soldering is finished, the splice can be removed from the mold. Low resistance value plus great accuracy in the dimensions can be achieved, which are requirements from the splice box design of this magnet. Additional benefits of this procedure are good repeatability and easier mechanical support for fixing the splices inside the connection box of the magnet.

V. Assembly and Impregnation

The assembly procedure and tooling will be briefly described here.

This process is schematically summarized in Fig. 8, where the detailed CAD pictures are shown. Fig. 8(a) shows the magnet after the winding step. It is in horizontal position as it was in the winding machine. The cables are held in position by means of the insulation tension and outer envelope, so special care must be taken during handling this assembly. It is transferred from the winding machine to the impregnation station with a crane until it is safely attached to the support. This supporting structure includes a mechanism to provide a fixed rotating axis to tilt the magnet into the vertical position with the crane (Fig. 8(b)). Then this position can be secured by additional blocking parts connecting diagonally to the structure.

The upper reservoir and the splices can be mounted and soldered at this moment, closing the whole volume to be impregnated. Previous similar designs were made with epoxy resin impregnation [6], while in this one, wax was selected given the promising results of this option for a CCT magnet ([7], [8]). Additional space for the wax reservoir is included in the Fig. 8(c)., and two additional parts hold the magnet at a medium height position for enhanced safety. The wax impregnation step will be done in this position, with proper thermal insulation and heaters in the outer surface. The cooling stage for the wax solidification will be made by means of forced air flow, with moving parts to allow the needed temperature gradient profile along the magnet. This is important as a previous work in a wax-impregnated CCT magnet has demonstrated [9]. The main point here is to make sure that no voids will be produced because of the different densities between liquid and solid phases of the wax, and the strategy is to allow a clear path of liquid wax between the solidification surface and the upper reservoir so that the upper hot wax from the reservoir can fill the empty space left by the solid wax during its phase change. The last picture Fig. 8(d) shows the finished magnet with its transportation structure, ready to be dismantled from the impregnation structure.

VI. Conclusion and Next Steps

The status of the fabrication of a combined function, straight canted cosine-theta prototype magnet for hadron therapy, in the scope of the IFAST project, has been presented.

The whole manufacturing procedure has been thoroughly considered. This approach was considered the best one in terms of robustness and risk control. The drawback is that some of the steps must be serialized. For instance, while the splices testing and winding tests can be done in parallel, the final manufacturing drawing for the mandrel cannot be considered finished until every detail of the process is fixed. Additional holes, pins, reference marks or any other detail that could be needed, for example, for the impregnation, must be included before machining the formers.

Once the testing phase was finished, every part and tooling were being manufactured.

Acknowledgment

The authors gratefully acknowledge Juan Carlos Perez, from CERN, for their help insights during the preparation of this work.

References

[1] A. Degiovanni and U. Amaldi, "History of hadron therapy accelerators," *Physica Medica*, vol. 31, no. 4, pp. 322–332, 2015, doi: 10.1016/j.ejmp.2015.03.002.R.

[2] F. Toral et al., "Status of Nb-Ti CCT magnet EU programs for hadron therapy," *IEEE Trans. Appl. Supercond.*, vol. 34, no. 5, Aug. 2024, Art. no. 4401705.

[3] E. DeMatteis et al., "Straight and curved canted cosine theta superconducting dipoles for ion therapy: Comparison between various design options and technologies for ramping operation," *IEEE Trans. Appl. Supercond.*, vol. 33, no. 5, Aug. 2023, Art. no. 4401205.

[4] J. Á. García-Matos et al., "Engineering design and fabrication of the nested orbit corrector prototype for HL-LHC," *IEEE Trans. Appl. Supercond.*, vol. 29, no. 5, Aug. 2019, Art. no. 4002205, doi: 10.1109/TASC.2019.2897233.

[5] R. Principe, S. Izquierdo-Bermudez, A. Milanese, H. Prin, S. Sgobba, and E. Todesco, "Development and qualification of high current splices and electrical connections for the HL-LHC magnets," *IEEE Trans. Appl. Supercond.*, vol. 34, no. 5, Aug. 2024, Art. no. 4800104, doi: 10.1109/TASC.2023.3335030.

[6] G. Montenero et al., "Coil manufacturing process of the first 1-m-long canted–cosine–theta (CCT) model magnet at PSI," *IEEE Trans. Appl. Supercond.*, vol. 29, no. 5, Aug. 2019, Art. no. 4002906, doi: 10.1109/TASC.2019.2897326.

[7] D. Barna et al., "Training-free performance of the wax-impregnated SuShi septum magnet," *Supercond. Sci. Technol.*, vol. 37, 2024, Art. no. 045006.

[8] D. Arbelaez et al., "Training-free demonstration of a 5.4 T Nb3Sn canted–cosine–theta accelerator dipole impregnated with paraffin wax," *Supercond. Sci. Technol.*, vol. 37, 2024, Art. no. 065015.

[9] D. Barna et al., "Test results of the first wax-impregnated Nb-Ti canted cosine theta septum magnet SuShi," *IEEE Trans. Appl. Supercond.*, vol. 34, no. 5, Aug. 2024, Art. no. 4003105, doi: 10.1109/TASC.2024.3354223.